High Resolution Analysis of the Secretory Pathway in Mammotrophs of the Rat Anterior Pituitary

MIRIAM M. SALPETER and MARILYN GIST FARQUHAR
Section of Neurobiology and Behavior, Division of Biology, Cornell University, Ithaca, New York 14850, and Section of Cell Biology, Yale University School of Medicine, New Haven, Connecticut 06510

ABSTRACT The secretory process in pituitary mammotrophs was analyzed by quantitative electron microscope autoradiography. Dispersed pituitary cells from estrogen-treated female rats were subjected to pulse-labeling with [^{3}H]leucine (5 min) followed by a chase incubation of up to 4 h. Autoradiograms were prepared using fine-grained emulsion (Kodak 129-01), and analyzed using a three-step "mask analysis' procedure: (*a*) the distribution of autoradiographic grains is determined as in a simple grain density analysis; (*b*) masks (transparent overlays) are used to generate expected grains from assumed sources; and (*c*) a computer program compares these two distributions and varies the expected distribution to match the observed distribution, thereby identifying the radioactive sources in the tissue.

The overall route of intracellular transport of prolactin from rough endoplasmic reticulum (ER) → Golgi complex → immature secretory granules → mature secretory granules was as established in previous studies. However, by use of the high resolution emulsion and method of analysis, the precision with which label could be localized within individual source compartments was much greater and the time resolution was much sharper than achieved previously using Ilford L4 emulsion and simple grain density analysis. The main new findings were as follows: (*a*) the ER was essentially drained of radioactivity by 30 min, the Golgi complex by 1 h, and the immature secretory granules by 2h postpulse. This indicates that the secretory product (prolactin) is rapidly and efficiently transported out of these compartments. (b) ~30% of the total radioactivity remains located in the ground cytoplasm over the entire postpulse period examined (up to 4 h), and by 30 min postpulse the grain density in the ground cytoplasm exceeded that of the ER. This indicates the ability to resolve ER-associated label (presumably associated mainly with secretory products) from the cytoplasmic label (presumably associated with nonsecretory proteins). (*c*) the specific activity of immature secretory granules was much greater than previously appreciated; at 1 h postpulse it was >200 times that of the adjacent Golgi complex cisternae. This large dynamic range in observed grain density demonstrates the ability to effectively correct for radiation spread and thus to detect with great accuracy high concentration of label even from very small structures (20–100 nm) which constitute a small percentage (<1%) of the total cell area.

The study of the intracellular synthesis and transport of secretory products was one of the earliest applications of electron microscope (EM) autoradiography to cell biology (3). By combining cell fractionation and EM autoradiographic procedures, the route of intracellular transport from endoplasmic reticulum (ER) → Golgi complex → secretory granules has been defined most carefully in the guinea pig pancreas (by Palade and coworkers [3, 11]) and subsequently in numerous other systems (e.g., 4, 8–10, 22). The autoradiographic studies have left several questions unresolved. Among them are the extent to which the radioactive profiles ascribed to various organelles are affected by radiation spread from adjacent structures and whether a cytoplasmic label, if present, can be distinguished from that in cell organelles. Furthermore, the decaying phase of the radioactivity in various organelles, especially in the rough ER, has been reported to be very slow (e.g., in the growth hormone secreting cells of the anterior pituitary [10] and in cells of the parotid [4]). The latter authors suggested

THE JOURNAL OF CELL BIOLOGY · VOLUME 91 OCTOBER 1981 240-246

that in the parotid this label may represent nonexportable protein remaining in the ER. Farquhar et al. (8) showed that in mammotrophs of the anterior pituitary some of the label seen over the ER was due to radiation spread from secretory granules. Yet such questions as whether any nonexportable radioactivity remains in the ER and/or the Golgi complex and how much label is ascribable to the cytoplasmic matrix remained unanswered.

These unresolved questions stem from technical difficulties in analyzing EM autoradiograms, mainly because there is a considerable amount of radiation spread from labeled structures due to limitations in the resolution of the preparation. Particularly bothersome is the fact that the percentage of developed grains falling outside a labeled organelle is inversely related to the size of that organelle (see references 15 and 16). Furthermore, because all cell organelles are embedded in the cytoplasmic matrix, mutual radiation spread between the cytoplasmic matrix and the organelles is inevitable. Many studies have ignored the fact that radioactivity in the ground cytoplasm can cause a significant overestimate of the developed grains ascribed to various organelles, especially if the latter are small and not heavily labeled.

The procedures for analyzing EM autoradiograms have been improving over the past ten years. These improvements stem from the utilization of studies on resolution to predict the grain distributions expected from variously labeled structures. By comparing these expected grain distributions with the observed grain distributions in an autoradiogram, the true sources can be identified, and their specific activities evaluated. Variants of this idea of analyzing EM autoradiograms by successive hypothesis testing have been published by Salpeter and co-workers (15, 17, 18), Blackett and Parry (1, 2), and Williams and Downs (23).

In this study, we used the mask analysis technique devised by Salpeter et al. (18) to analyze autoradiograms of dissociated mammotrophs or prolactin-secreting cells of the rat pituitary after pulse labeling with [^{3}H]leucine. The secretory process has been well studied both by cell fractionation (reviewed in references 5 and 24) and by EM autoradiography (8) in these cells. It therefore constitutes a good model system for examining what new information the improved procedures for analyzing autoradiograms can provide. Our main goals were to determine more quantitatively than previously reported the time-course of drainage of secretory products from the cellular organelles and to resolve the secretory product from the nonexportable pool. We present results which show that this is indeed achievable with our method of analysis.

MATERIALS AND METHODS

Preparation of Cells

Cells dissociated from estrogen-treated female rat pituitary glands were pulse-labeled for 5 min at 37°C with L-[4,5-^{3}H]leucine (55 Ci/mmol from Schwarz/Mann) as previously described (8). At the end of the pulse, one aliquot (to be referred to as the 5-min time-period) was diluted with 1 cc of cold chase medium containing an excess (× 10) of nonlabeled leucine to stop incorporation. The remaining material was overlaid over 4% bovine serum albumin, spun for 5 min at 70 *g* at 37°C and then resuspended in 10 ml of chase medium and incubated up to 4 h. Aliquots were then removed at 0.5, 1, 2, 3, and 4 h intervals (timed after the beginning of the pulse), put into ice-cold chase medium, centrifuged, fixed in Karnovsky's OsO_4 fixative, postfixed in OsO_4, stained in 5% uranyl acetate, and embedded in Epon as previously described (8).

Preparation of Autoradiograms

Autoradiograms were prepared by the "flat substrate" procedure of Salpeter and Bachmann (14, 16), using 1,000 Å sections and monolayers (pale gold) of the NTE-type fine-grain emulsion known as Kodak 129-01 (Eastman Kodak, Rochester, N. Y.) (19).[1] Development was with Dektol (2 min at 24°C). For our experimental conditions (using ^{3}H-labeling, 1,000 Å stained sections and the NTE-type emulsion) the half-distance resolution (HD) is 1,000 Å (15).[2] Because sensitivity for the 129-01 emulsion is variable from batch to batch and changes with time, we tested the sensitivity before coating any sections, and, based on the value obtained, adjusted the exposure time (usually 6–10 d) so that all the different experimental samples would have an equivalent grain yield. In addition, several emulsion layers were exposed to a sensitivity test specimen were always stored together with the experimental slides and developed at the same time as the latter to determine whether any change in sensitivity had occurred during the exposure period. Some autoradiograms were exposed for shorter periods (2–3 d), and the linearity of the grain yield with time was checked to determine whether saturation of the emulsion was occurring over very hot structures.

Autoradiograms were scanned in a Philips 301 microscope, and only prolactin cells were photographed, magnified to a final magnification of × 25,000 and printed on 11 x 14 paper.

Analysis of Autoradiograms

The autoradiograms were analyzed using the "mask" analysis method described by Salpeter et al. (18), which is similar to the method of Blackett and Parry (2). It consists of three basic steps: (1) tabulation of the distribution of observed grains in the autoradiograms; (2) use of "masks" (transparent overlays) to generate expected grain distributions which take into account the resolution limiting radiation spread around assumed sources in the specimen; and (*c*) use of a computer program to compare the two distributions and vary the relative radioactivity in the different assumed sources until a best fit (minimum chi-square) is obtained between the expected and observed distributions.

By definition, if a compartment is used to tabulate the location of either observed or generated (expected) grains, it is called a "grain compartment." If it is used to tabulate the location of mask sources, it is called a "source compartment."

TABULATION OF DEVELOPED (OBSERVED) GRAINS: The location of each developed grain was determined as in the simple grain density method (17). A hole was punched by a needle through the print at the center of the smallest circle that could circumscribe that grain, and the grain compartment over which the grain centers fell was then tabulated.

TABULATION OF GENERATED (EXPECTED) SOURCE TO GRAIN MATRIX: This analysis used the "masks" as previously described (18). The masks contain a random set of source-to-grain pairs each consisting of a source (center of a small circle) connected by a line to the center of an "X" representing a grain expected from that source. Each expected grain is centered in a circle of 1-HD radius. The distance from the expected grain to the source was chosen randomly from among a set of ten distances, each with an equal probability of occurring from a point source (calculated on the basis of the resolution studies of Salpeter et al. [15]). When such masks are matched to the resolution of a specimen and the magnification of the print, they can be used to derive the expected grain distribution due to radiation spread between various interspersed compartments in that autoradiogram by overlaying the autoradiographic print, and determining the location of each source-to-grain pair. Accordingly, for this study, the set of six masks (18) were reproduced at × 25,000 to match the magnifications of the prints (i.e., the 10-HD bar on the mask was magnified to 25 mm, because the HD for our specimen was 1000 Å [15]). All six masks were taped together to make one large composite "mask" (72 source-grain pairs), which fits the size of the large print.

For each source-to-grain pair, the location of the source (source compartment) and expected grain (grain compartment) was marked, and the set tabulated in matrix form (as, e.g., in Fig. 2, where the grain compartments are listed across and the source compartments down). If the source of a pair fell on a mitochondrion and the generated (expected) grain on the Golgi complex cisternae, this source-to-grain pair would be tabulated in the matrix element, seventh row, third column of Fig. 2.

If one sums each matrix row across, one gets the total number of the tabulated source points that fell into each source compartment, and thus the relative area occupied by the source compartment. If one sums each column down, one gets all the generated grains that fell into a given grain compartment, and thus the relative area of that grain compartment.

---

[1] The commercial batches of Kodak 129-01 used in this study had a lower sensitivity (by about two and a half times) than that reported by Salpeter and Szabo (19).

[2] HD was defined as the distance from a radioactive line source which contains 50% of the developed grains derived from the source.

INITIAL ANALYSIS: We performed an initial analysis to identify the labeled structures and to obtain a general value for intercellular background. For this initial analysis, each print was analyzed using the above described composite "mask" in only one position (called position 1, top left of mask aligned with top left of print). The grain and source compartments used were the nucleus (N), endoplasmic reticulum (ER), Golgi complex cisternae (GOL/C) vesicles (GOL/V), immature granules (GR/IM), mature granules (GRM), ground cytoplasm (CYT), mitochondria (MIT), cytoplasmic vesicles or vacuoles, background between cells, and other cells. In this initial tabulation, the size of each of the smaller grain compartments (ER, Golgi complex cisternae and vesicles, and immature granules) was increased by a 1-HD rim to include the bulk of the grains scattered by radiation spread and thus to quickly gain a better assessment of which compartments were labeled.

From the initial tabulation, we found that: (*a*) the grain density over the nucleus was not above that of the intercellular background (~0.07 grains/μm^2); (*b*) the various cytoplasmic vesicles and vacuoles were also essentially unlabeled during the time periods tabulated; (*c*) the label in mitochondria was variable but similar to that in the cytoplasm; (*d*) the label in Golgi complex vesicles was similar to that in Golgi complex cisternae; and (*e*) the two secretory granule compartments showed prolonged periods of high label. Accordingly, for the final analysis, we either pooled or omitted some of the compartments (*a-d*) (see below), and we subdivided the secretory granules into three groups, rather than two, which we called immature, intermediate, and mature as follows: the immature granules (GRA) were small (20–100 nm), located near the stacked Golgi complex cisternae and had a space between the membrane and its dense core; the intermediate granules (GRB) contained multiple condensing cores or were dumbbell-shaped; and the mature granules (GRM) were single, somewhat larger, usually circular or only slightly pear-shaped. These groups consist of Type I, Type II and III, and Type III and IV granules as defined in reference 8.

FINAL GRAIN COMPARTMENTS USED FOR TABULATION OF OBSERVED AND GENERATED GRAINS: Based on the initial analysis, the final grain compartments selected included the following. (*a*) Compartment 1 contains rough ER (called ER/IN which consisted of the ER lumen and limiting membrane); however, when the ER was within 2 HD of a secretory granule, a separate ER + GR grain compartment was tabulated (e.g., see compartment 6 below). (*b*) Compartment 2 contains a rim of 1-HD width around all ER profiles (called ER/OUT). (*c*) Compartment 3 contains the Golgi complex cisternae plus a 1-HD rim around these profiles (GOL/C), except when the Golgi complex cisterna was within 2 HD of a secretory granule, in which case a separate compartment was tabulated (e.g., see compartment 7 below). (*d*) Compartment 4 contains immature granules (GRA/IN). (*e*) Compartment 5 contains a 2-HD rim around all immature granules (GRA/OUT). (*f*)When the 2-HD rim around an immature granule overlapped ER, compartment 6 constituted a separate compartment (called GRA + ER).[3] (*g*) When the 2-HD rim around an immature granule overlapped a Golgi complex cisterna, compartment 7 constituted a separate compartment (called GRA + Gol). (*h*) Compartments 8–11 are the same as compartments 4–7, but for the intermediate granules (GRB). (*i*) Compartments 12–15 are the same as 4–7, but for mature granules (GRM).[3] (*j*) Compartment 16 contains ground cytoplasm (CYT) (because of the 1- to 2-HD rims around many organelles as described above, the "ground cytoplasm" grain compartment was separated from the organelles by these rim compartments); (*k*) Compartment 17 contains background between cells. Because some of the grain compartments could overlap (e.g., ER/OUT and GOL/C), whenever a grain center fell within more than one of the above defined grain compartments, partial credit was given.

FUNCTION OF RIM COMPARTMENTS: The rim compartments (e.g., ER/OUT or GR/OUT) as well as the pooled compartments (e.g., GR + ER or GR + Gol) have several functions (18): (*a*) they provide a buffer zone between very heavily labeled structures and their less radioactive neighbors (most important when there are small heavily labeled structures, as in this study). (*b*) They provide a check on the accuracy of the source designation because of the fact that the expected distribution around a source has a characteristic shape (as illustrated by the universal curves [15] and the relative number of grains in these grain compartments must conform to that of the universal curves). If the source compartments are not correctly chosen an insufficient Chi-square minimization will be achieved.

FINAL SOURCE COMPARTMENTS: Based on the initial analysis, the following source compartments were defined: Golgi complex cisternae (GOL/C), rough ER, immature (GRA), intermediate (GRB), and mature granules (GRM), ground cytoplasm and vacuoles (CYT), and intercellular material and background. Since the nucleus had a low grain density, it was eliminated, as was a 2-HD rim around the nuclear envelope to eliminate any possible effect of radiation spread from the nucleus onto other compartments. Other cell types (other than mammotrophs) were also eliminated as was a 2-HD rim around them, again to minimize the effect of radiation spread from this eliminated source. The intercellular background was recorded, but treated separately for comparison with the cellular compartments.

GENERATION OF FINAL EXPECTED SOURCE TO GRAIN MATRIX: For each print, the mask overlay was first used in one of the 36 different positions described below; the source and grain assignments made for each source-to-grain pair, and recorded in its matrix element similar to that in Fig. 2. The size of the data pool was enhanced for sources with a small overall area (which included the secretory granules) as follows: for each print, the "masks" were used in all the additional positions and only those "source-to-grain" pairs whose sources fell on the small source compartments in question were tabulated. The matrix row obtained from these enhanced source tabulations was subsequently divided by the enhancement factor (i.e., the number of times the masks were used for the tabulation of the enhanced compartments divided by the number of times they were used for recording all compartments in the print).

The possible total number of different mask positions was 36. These included aligning the two opposite corners of the mask with the upper left corner of the print, mirror imaging the mask for these two positions, or shifting the masks to the right and/or down by increments equal to one-third the source spacing (i.e., 11 mm at this magnification). Because the source distribution in each mask (illustrated in reference 18) is not centered, rotating or moving the mask places the sources in a different position relative to the cellular organelles, and also varies the direction of the grains relative to the sources.

By these manipulations, a source-to-grain matrix could be generated to fulfill the criteria laid down in reference 18 for adequate statistical analyses, i.e., that there should be a total of five times as many generated grains tabulated as observed grains and for each grain compartment there should be at least three times as many generated grains tabulated as observed grains.

COMPUTER ANALYSIS: A computer program for chi-square minimization (as described in the appendix of reference 18) was then used to compare the generated with the observed distributions, to find the best fit between the two and to identify most likely distribution of radioactive sources in the tissue (e.g., Fig. 3). This is accomplished as follows: Each matrix row is multiplied by different multiplying factors, and, for each set of multiplying factors, the resultant summed generated grains in each grain-compartments column is compared (by chi-square) with the observed grains in these same grain compartments. The multiplying factors are varied in small increments until a minimum chi-square value is obtained. If, once the chi-square is minimized, the observed and expected distributions are well matched, i.e., not significantly different (degrees of freedom is given by the number of grain compartments minus the number of source compartments), then the multiplying factors give the most likely relative distribution of radioactivity in the various source compartments. If even with the lowest chi-square, the generated distribution is still significantly different from the observed distribution, it indicates (as was discussed above) that either the source compartments were incorrectly defined or there is some error in the grain tabulation. Then, a more careful grain tabulation is required or new source-to-grain matrix (step 2, see Analysis of Autoradiograms) must by generated using different source compartments.

RESULTS

Fig. 1 gives a typical EM autoradiogram of a mammotroph fixed 30 min postpulse. Fig. 2 gives a sample of the tabulation of the observed grain distribution and generated source-to-grain matrix obtained from the autoradiograms 2 h postpulse, and Fig. 3 gives a typical computer printout for the analysis of the sample data in Fig. 2. The latter illustrates the form in which the computer program provides for each source compartment a value for relative radioactivity, called "optimized source distribution" which is essentially the final grain density, corrected for radiation spread. The final optimized source distributions for each time-point are given in Table I. The values represent the grain densities (grains per unit area of grain compartment) which would be obtained by a simple density analysis (17) if there were perfect resolution and thus no radiation spread. Table II presents the contribution from each compartment (corrected grain density times relative area) to the overall activity of the entire cell, expressed as percent of total grain density. Figs. 4 and 5 present smoothed curves of the information from Tables I and II, respectively. For each time-point, a value was chosen from within the entire error

[3] These special rim compartments GR + ER and GR + GOL were used only during those postpulse periods when the relevant granule was heavily labeled.

range to produce such a smooth curve. Because we were primarily concerned with the drainage of material from the secretory compartments, we omitted a fine time resolution of the period between 5 and 30 min postpulse. We therefore do not have an accurate value for the peak grain density in the ER, which appears to occur before 5 min, nor for that in the Golgi complex cisternae, which was previously shown to occur at ~15 min postpulse [8].

The results (Fig. 4) demonstrate the same overall secretory pathway (rough ER → Golgi complex → immature → intermediate → mature granules) as reported previously using Ilford L4 emulsion and simple grain density analysis (8). However, in general, the precision with which label could be localized within individual source compartments was much greater than achieved previously, and the time resolution was much sharper. Accordingly, the new findings provided by our data are as follows: (*a*) The grain density dropped essentially to zero in the ER by 30 min, in the Golgi complex by 1 h, and in the immature granules by 2 h postpulse, leaving no significant residual radioactive material in any of these three compartments (Table I and Fig. 4). (*b*) The grain density (see Table I) in the immature granules (GRA) was far higher, relative to the label in adjacent organelles, than noted previously; at 30 min postpulse it was 100-fold and at 1 h almost 200-fold higher than in the nearby Golgi complex cisternae (82.8 vs. 0.7, and 19.3 vs. 0.1, respectively). (*c*) The peak total radioactivity or

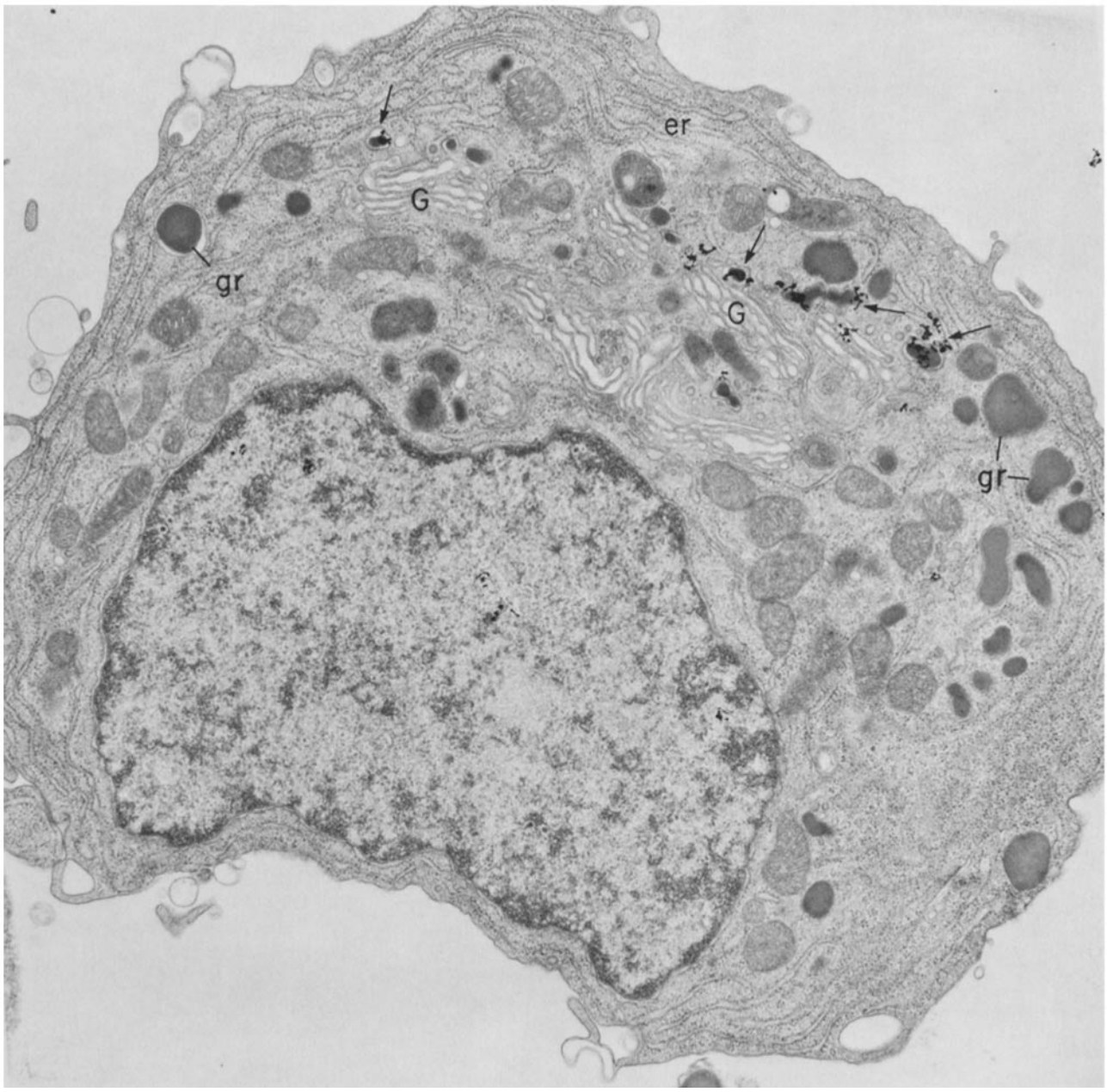

FIGURE 1 Sample electron microscope autoradiogram of a mammotroph or prolactin cell from a cell suspension prepared from estrogen-treated rat-pituitaries culture overnight, pulsed for 5 min with [^{3}H]leucine (500 μCi/ml), and fixed after a 30-min chase incubation. Thin sections were coated with Kodak 129-01 emulsion, exposed for 2-6 d and developed in Dektol. Most of the autoradiographic grains are located over immature granules (arrows) in the Golgi apparatus region close to the stacked Golgi apparatus cisternae (*G*). Mature granules (*gr*) are essentially unlabeled at this time. × 18,000

OBSERVED GRAIN DISTRIBUTION

ER/IN	ER/OUT	GOL/C	GOL/V	GRA/IN	GRA/OUT	GRB/IN	GRB/OUT	GRB+ER	GRM/IN	GRM/OUT	MIT	CYT
8.00	25.50	15.50	11.00	3.00	8.50	191.00	93.00	6.50	27.00	32.80	13.00	37.00

GENERATED SOURCE TO GRAIN MATRIX (GRAIN COMP ACROSS)

	ER/IN	ER/OUT	GOL/C	GOL/V	GRA/IN	GRA/OUT	GRB/IN	GRB/OUT	GRB+ER	GRM/IN	GRM/OUT	MIT	CYT
ER	34.50	35.00	1.50	1.00	0.0	2.00	1.00	5.00	3.00	3.00	19.00	6.00	5.00
GOL/C	0.0	2.50	43.50	11.00	0.0	4.00	0.0	1.00	0.0	0.0	3.00	0.0	1.00
GOL/V	0.0	1.50	13.00	24.00	1.00	9.00	1.00	2.00	0.0	1.00	2.00	0.50	0.0
GRA	0.20	0.20	0.40	0.50	1.10	2.70	0.0	0.10	0.0	0.0	0.10	0.0	0.20
GRB	0.38	0.43	0.18	0.03	0.20	0.16	11.90	5.10	0.40	0.73	1.19	0.34	0.43
GRM	0.30	1.10	0.80	0.40	0.0	0.10	1.70	0.50	0.0	25.20	14.40	9.00	1.50
MIT	3.00	6.00	3.00	1.00	2.00	2.00	1.00	2.00	0.0	1.00	5.00	46.00	2.00
CYT	37.50	97.00	17.50	17.00	2.00	3.00	7.00	23.00	2.50	15.00	49.50	29.00	111.00

FIGURE 2 Sample (computer printout) of observed grain distribution and generated source-to-grain matrix obtained from autoradiograms at 2-h postpulse. The observed grain distribution was obtained by locating the center of each observed grain and assigning it to a grain compartment as defined in the methods section. The generated source-to-grain matrix was obtained by assigning each "source-to-grain" pair to its appropriate matrix element; e.g., if the source of a pair fell on an intermediate granule (*GRB*) and the grain of the pair fell on the lumen of the ER (*ER/IN*), the pair would be located in the fifth row, first column. The sum of each matrix row (across) thus represents all generated grains derived from one source compartment and scattered into all the various grain compartments. The sum of each column (down) represents the generated grains derived from all the source compartments which fell into one grain compartment. The matrix rows for the three granule compartments were obtained by using each mask in 12 different positions. The values given here for these rows are one-twelfth of the total data collected, to keep the unit source density constant for all the sources.

OPTIMIZED SOURCE DISTRIBUTION WITH EACH DENSITY ≥ ZERO

ER	GOL/C	GOL/V	GRA	GRB	GRM	MIT	CYT
0.0	0.1257	0.2317	0.6417	16.0461	0.3955	0.0	0.2043

ERROR RANGES OF VARIABLE SOURCE DENSITIES

0.1217	0.1155	0.1781	1.0533	0.9836	0.1896	0.0952	0.0491

COMPUTED GRAIN DISTRIBUTION FOR OPTIMIZED SOURCES

ER/IN	ER/OUT	GOL/C	GOL/V	GRA/IN	GRA/OUT	GRB/IN	GRB/OUT	GRB+ER	GRM/IN	GRM/OUT	MIT	CYT
14.01	27.94	15.51	11.38	4.56	7.54	193.28	87.38	6.93	24.98	35.81	15.06	30.42

COMPONENTS OF CHI-SQUARE FOR EACH GRAIN COMPARTMENT

2.575	0.213	0.000	0.012	0.531	0.122	0.027	0.361	0.027	0.164	0.253	0.281	1.421

TOTAL CHI-SQUARE

5.987

FIGURE 3 Computer analysis for data as seen in Fig. 2. The *optimized source distribution* refers to the best multiplying factor for each of the source compartments listed across. These values were not allowed to become negative (thus, ≥0). The *error ranges of variable source densities* were calculated for each of the above listed source compartments by an algorithm given in reference 18. This considers the fact that the number of developed grains (N) in an autoradiogram have a Poisson distribution. The final error range is calculated so that if the observed grain value in any grain compartment would vary by the likely deviation of $\pm\sqrt{N}$, the resultant optimized source density would still fall within the computed error range. The *computed grain distribution for optimized sources* gives for each of the grain compartments listed across, the expected grains which result from summing the generated grains in each compartment after each matrix row is multiplied by the multiplying factor given in "optimized source distribution" above. The *components of chi-square for each grain compartment* is the chi-square value obtained by comparing the expected grains in each grain compartment (listed above) with the observed grains in that grain compartment (given in Fig. 2). The *total chi-square* is the sum of all the individual chi-square values. A chi-square of 5.987 means that the observed and expected distributions are not significantly different (P = >0.25 degrees of freedom is given by the number of grain compartments minus the source compartments = 5). The *optimized source distribution* is thus the corrected grain density for each source compartment, i.e., the grain density which would be obtained from these sources if there were no radiation spread.

TABLE I

*Corrected Grain Density**

	Source compartments (percent area)‡						
Time after pulse label	ER (20%)‡	Golgi complex cisternae (9%)	GRA (0.8%)	GRB (4%)	GRM (8%)	CYT (57.6%)	Total grain density§
5 min	0.95 ± 0.2	2.1 ± 0.4	2.6 ± 1.8	0.0 ± 0.5	0.3 ± 0.45	0.5 ± 0.1	0.80
30 min	0.0 ± 0.1	0.7 ± 0.2	82.8 ± 6.5	0.15 ± 0.2	0.25 ± 0.2	0.2 ± 0.05	0.61
1 h	0.0 ± 0.1	0.1 ± 0.1	19.3 ± 1.7	5.7 ± 0.4	0.45 ± 0.15	0.2 ± 0.05	0.56
2 h	0.0 ± 0.1	0.1 ± 0.1	0.6 ± 1.0	16.0 ± 1.0	0.4 ± 0.2	0.2 ± 0.05	0.77
3 h	0.0 ± 0.2	0.1 ± 0.1	1.6 ± 1.0	7.6 ± 0.7	1.45 ± 0.2	0.4 ± 0.1	0.67
4 h	0.1 ± 0.1	0.15 ± 0.1	0 ± 0.6	0.8 ± 0.2	1.55 ± 0.2	0.25 ± 0.05	0.37

* The values for corrected grain density (i.e., optimized source distributions obtained from computer printouts as in Fig. 3). It represents what the grains per unit area of each source would be if there were no radiation spread, i.e., perfect resolution. Unit area in all cases is given by the spacing in the mask, which was 1.8 μm^2 in this study. The emulsion background was ~0.03/μm^2. Between 700 and 1,500 grains and ~1,500 μm^2 of tissue were analyzed for each time point.

‡ The percent area given for each compartment is the average over all postpulse periods.

§ Total grain density is grains from all compartments/total area tabulated. The error ranges (e.g., Fig. 3) given for individual compartments represent uncertainties due to radiation spread and Poisson statistics in the grain sampling (which is negligible for the total density). However, for each time period, we estimate an additional ~20% uncertainty due to variations in the autoradiographic and other experimental procedures.

TABLE II

Relative Distribution of Radioactivity

Time after pulse label	Percent activity*					
	ER	Golgi complex cisternae	GRA	GRB	GRM	CYT
5 min	24.3 ± 5.0	26.8 ± 5.0	2.7 ± 1.8	0.0 ± 2.4	2.2 ± 3.0	44.0 ± 8.7
30 min	0.0 ± 2.6	9.3 ± 2.7	68.7 ± 5.1	0.7 ± 0.9	1.2 ± 1.6	23.0 ± 5.8
1 h	0.0 ± 2.9	1.5 ± 1.7	28.6 ± 2.5	39.0 ± 2.7	5.7 ± 1.8	25.2 ± 6.2
2 h	0.0 ± 2.6	1.6 ± 1.6	0.7 ± 1.2	75.4 ± 4.7	4.4 ± 2.3	18.0 ± 4.5
3 h	0.0 ± 5.6	1.6 ± 1.6	1.6 ± 1.0	35.0 ± 3.2	21.9 ± 3.0	39.8 ± 10.2
4 h	4.7 ± 4.7	3.7 ± 3.7	0.0 ± 1.1	7.7 ± 1.8	37.0 ± 5.1	44.8 ± 8.8

* Obtained from the "corrected grain density" (Table I) times relative area and expressed as a percent of total grain density. The "relative area" used to obtain these percent values was derived separately from the autoradiograms from each postpulse time-point and not from the average value given in Table I. Any discrepancy between the values given here and that which can be calculated directly from the data in Table I is due to fluctuations in the percent area occupied by the organelles in the autoradiograms for different postpulse experiments, which for the small compartments varied by as much as a factor of 2.

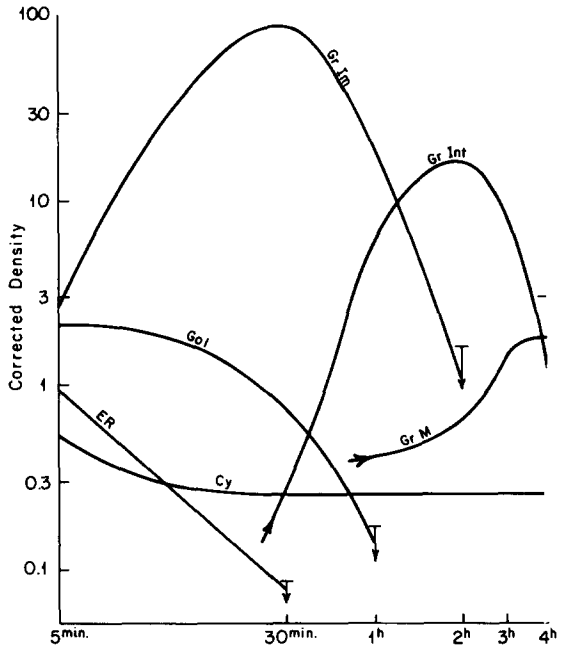

FIGURE 4 Smoothed curve giving optimized source distribution (grain densities) for the different time periods in this study (x-axis) (based on data from Table I). Since this study looked in detail at the drainage of the secretory products at >30 min postpulse, we do not mean to imply that the smoothed curve for the Golgi apparatus compartment accurately represents the peak value in this compartment, known to occur ~15 min postpulse (8). (Emulsion background in these units was 0.037. The grain density in the intercellular space and in the nucleus was 0.1.) Arrows indicate the time when our data give only an upper limit to the value, since (given the error range) it is not significantly different from zero.

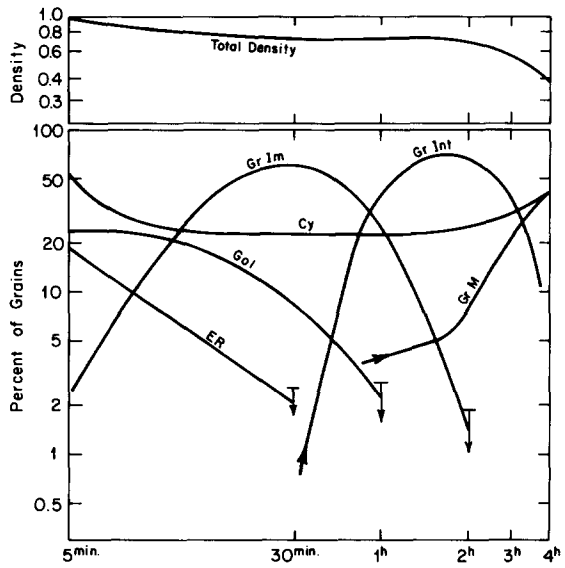

FIGURE 5 Data derived from Tables I and II. Top gives total density (grains/entire area tabulated) normalized to 1 at 5 min. Bottom gives activity in each compartment expressed as percent of total activity at each time postpulse. Arrows are used as in Fig. 4.

peak density times relative area (Table II) was essentially the same in the immature granules (at 30 min) as in the intermediate granules (at 2 h) (~69% and 75%, respectively). This suggests that there is a total transfer of material from the immature to the intermediate granules with no loss of material from the immature granules to any other compartment and no input into the intermediate granules from any source other than immature granules. (*d*) The intermediate granules (GRB) have a 5-fold larger volume (4% vs. 0.8%) (Table I) and about threefold longer drainage time than do the immature granules. The time for the radioactivity to decrease to half its peak value for the immature granules is calculated to be ~20 min compared to 1 h for the intermediate granules (Fig. 4). Thus, the conversion of immature to intermediate granules is faster than the conversion of intermediate to mature granules. This explains why, after a brief pulse label, some intermediate and mature granules (~10–30%) are very heavily labeled while others had no label associated with them at all. Thus, the inhomogeneity of label among intermediate and mature granules reflects both intracellular processing and storage. (*e*) A considerable amount of radioactivity (~30% of the total) persists in the ground cytoplasm over the entire period tabulated (Table II). By 30 min postpulse, the cytoplasmic grain density exceeded that in the ER.

DISCUSSION

Using a well-characterized (5, 7, 8, 20, 21, 24) secretory cell model (i.e., the prolactin cell or mammotroph of the rat anterior pituitary), we have applied an improved autoradiographic methodology which involves fine-grained emulsion and an analysis which corrects for radiation spread to determine the fate of newly synthesized secretory and nonsecretory proteins. Our data indicate that after a pulse label with [^{3}H]amino acids, the radioactive proteins (presumably associated mainly with

prolactin) are transported through the secretory compartments more efficiently than previously reported (8). The radioactive material is drained from the rough ER to the Golgi complex by 30 min, from the Golgi complex to immature secretory granules by 1 h, and from the immature to intermediate granules by 2 h, leaving essentially no radioactive material in these compartments. Residual nonexported material is located in the ground cytoplasm, not in the ER, as previously suggested for parotid cells (4) and for somatotrophs of the anterior pituitary (10).

According to the accepted model for the intracellular transport and processing of secretory proteins (12, 13), once packaged into secretory granules, secretory products are retained in this compartment without further input or loss until they are discharged extracellularly by exocytosis or destroyed intracellularly by crinophagy (5, 20). If correct, this model predicts that the total radioactivity should be the same at the peak time in successive granule compartments and the residence time of the packaged material in a given compartment should be proportional to the volume of that compartment. The latter prediction should be corrected for further concentration, if and when it occurs. Our data are compatible with this model at times before a significant (<10% [21]) overall loss of secreted material from the cell (i.e., at <2 h), in that the percent total activity (grain density times percent of area) at their respective peak times for immature and intermediate granules is virtually the same (69 ± 5 at 30 min postpulse for immature and 75 ± 5 at 2 h postpulse for intermediate granules) (see Table II). From the ratios of relative volumes of immature and intermediate granules (0.8% vs. 4%) and half-time of decays in radioactivity (20 min vs. 1 h) (see Results), it is clear that a major delay occurs during the intermediate granule stage because there is a three- to five-fold increase in both the volume and half-time of decay in this compartment over the immature granules. This is presumably the time required for conversion of intermediate to mature granules under our conditions (estrogen-treated mammotroph in suspension culture). The further increase in volume by about two times in the mature granules suggests a further delay in that compartment; however, our study was not extended long enough in time to assess the drainage time of radioactivity from that compartment. As pointed out in an earlier investigation (8), the marked heterogeneity of label in intermediate and mature granules indicates that once a granule is formed, there is no mixing (by fusion) of its contents with that of other granules.

The power of the approach used in this study is illustrated in its ability to resolve a high concentration of label in small structures such as the immature granules. Each immature granule is only 20–100 nm in diameter, and in total, they constitute <1% of the entire cell area. Moreover, they are typically located close to the stacked Golgi complex cisternae. The successful resolution of the label between these two closely associated compartments, accomplished primarily by the use of special rim (e.g., ER/OUT) and pooled grain compartments, (e.g., GR + ER), demonstrates the potential usefulness of this approach for investigating a number of other still unresolved questions pertaining to intracellular traffic, such as the pathways taken by secretory proteins and membrane proteins to and through the Golgi complex (6) and pathways taken by recycling membrane from the cell surface to other cell compartments (7). Moreover, by accurately correcting for radiation spread so that the total activity in a compartment can be assessed, it is further possible to study the rate of drainage of material from one compartment to the next and, thus, to study the influence of various factors which control or influence secretion and to pinpoint with greater accuracy the site of the effect. Finally, the ability to resolve the ground cytoplasm from the lumen of the ER makes it possible to use EM autoradiography to study early stages of protein synthesis and to determine the relative amount and role of cytoplasmic label in different cells.

We wish to thank Edwin Salpeter for helpful discussions and Maria Szabo, Joyce Davis, and Bonnie Peng for technical assistance.

This work was supported by grants GM 10422 (to M. M. Salpeter) and AM 17780 (to M. G. Farquhar) from the National Institutes of Health.

Received for publication 23 July 1980, and in revised form 4 May 1981,

REFERENCES

1. Blackett, N. M., and D. M. Parry. 1973. A new method for analyzing electron microscope autoradiographs using hypothetical grain distributions. *J. Cell Biol.* 57:9–15.
2. Blackett, N. M., and D. M. Parry. 1977. A simplified method of "Hypothetical Grain" analysis of electron microscope autoradiographs. *J. Histochem. Cytochem.* 25(3):206–214.
3. Caro, L., and G. E. Palade. 1964. Protein synthesis, storage, and discharge in the pancreatic exocrine cell. An autoradiographic study. *J. Cell Biol.* 20:473–495.
4. Castle, J. D., J. D. Jamieson, and G. E. Palade. 1972. Radioautographic analysis of the secretory process in the parotid acinar cell of the rabbit. *J. Cell Biol.* 53:290–311.
5. Farquhar, M. G. 1977. Secretion and crinophagy in prolactin cells. *In* Comparative Endocrinology of Prolactin. H D. Dellman, J. A. Johnson, and D. M. Klachko, editors. Plenum Press, Inc., New York. 37–94.
6. Farquhar, M. G. 1978. Traffic of products and membranes through the Golgi complex. *In* Transport of Macromolecules in Cellular Systems. S. Silverstein, editor. Dahlem Konferenzen, Berlin. 341–362.
7. Farquhar, M. G. 1980. Membrane recycling in secretory cells: implications for traffic of products and specialized membranes within the Golgi complex. *In* Basic Mechanisms of Cellular Secretion. A. Hand and C. Oliver, editors. Academic Press, Inc., New York. In press.
8. Farquhar, M. G., J. J. Reid, and L. W. Daniell. 1978. Intracellular transport and packaging of prolactin: a quantitative electron microscope autoradiographic study of mammotrophs dissociated from rat pituitaries. *Endocrinology.* 102:296–311.
9. Howell, S. L., M. K. Kostianovsky, and P. E. Lacy. 1969. Beta granule formation in isolated islets of Langerhans: a study by electron microscopic radioautography. *J. Cell Biol.* 42:695–705.
10. Howell, S. L., and M. Whitfield. 1973. Synthesis and secretion of growth hormone in the rat anterior pituitary. I. The intracellular pathway, its time course and energy requirements. *J. Cell Sci.* 12:1–21.
11. Jamieson, J. D., and G. E. Palade. 1967. Intracellular transport of secretory proteins in the pancreatic exocrine cell. *J. Cell Biol.* 34:577–615.
12. Jamieson, J. D., and G. E. Palade. 1977. Production of secretory proteins in animal cells. *In* International Cell Biology, 1976–1977. B. B. Brinkley and K. R. Porter, editors. The Rockefeller University Press, New York. 326–336.
13. Palade, G. E. 1975. Intracellular aspects of the process of protein secretion. *Science (Wash. D. C.).* 189:347–358.
14. Salpeter, M. M., and L. Bachmann. 1964. Autoradiography with the electron microscope. A procedure for improving resolution, sensitivity, and contrast. *J. Cell Biol.* 22:469–477.
15. Salpeter, M. M., L. Bachmann, and E. E. Salpeter. 1969. Resolution in electron microscope radioautography. *J. Cell Biol.* 41:1–20.
16. Salpeter, M. M., and L. Bachmann. 1972. Electron microscope autoradiography. *In* Principles and Techniques of Electron Microscopy: Biological Applications. Vol. II. M. A. Hayat, editor. Van Nostrand Reinhold, New York. 221–278.
17. Salpeter, M. M., and F. A. McHenry. 1973. Electron microscopy autoradiography. Analysis of autoradiograms. *In* Advanced Techniques in Biological Electron Microscopy. J. K. Koehler, editor. Springer-Verlag, New York. 113–152.
18. Salpeter, M. M., F. A. McHenry, and E. E. Salpeter. 1978. Resolution in electron microscope autoradiography. IV. Application to analysis of autoradiographs. *J. Cell Biol.* 76:127–145.
19. Salpeter, M. M., and M. Szabo. 1976. An improved Kodak emulsion for use in high resolution electron microscope autoradiography. *J. Histochem. Cytochem.* 24:1204–1206.
20. Smith, R. E., and Farquhar, M. G. 1966. Lysosome function in the regulation of the secretory process in cells of the anterior pituitary gland. *J. Cell Biol.* 31:319–347.
21. Walker, A. M., and Farquhar, M. G. 1980. Preferential release of newly synthesized prolactin granules is the result of functional heterogeneity among mammotrophs. *Endocrinology.* 107:1095–1104.
22. Weinstock, M., and C. P. Leblond. 1974. Synthesis, migration, and release of precursor collagen by odontoblasts as visualized by radioautography after [^{3}H]proline administration. *J. Cell Biol.* 60:92–127.
23. Williams, M. A., and A. Downs. 1978. An iterative approach to the analysis of EM autoradiographs. *J. Microsc. (Oxf.).* 114(2):157–178.
24. Zanini, A., G. Giannattasio, and J. Meldolesi. 1980. Intracellular events in prolactin secretion. *In* Synthesis and Release of Adenohypophyseal Hormones. M. Jutisz and K. W. McKerns, editors. Plenum Press, Inc., New York. 105–123.